ACS APPLIED MATERIALS & INTERFACES

Research Article

www.acsami.org

Graphene-Enveloped Poly(*N*-vinylcarbazole)/Sulfur Composites with Improved Performances for Lithium−Sulfur Batteries by A Simple Vibrating-Emulsification Method

Guoxing Qu,[†,‡,§] Jianli Cheng,[†,‡] Xiaodong Li,[‡] Ling Huang,[‡] Wei Ni,[‡] Zhiyu Wang,[‡] and Bin Wang*[,‡]

[‡]Institute of Chemical Materials, China Academy of Engineering Physics, Mianyang, Sichuan 621900, China

[§]College of Chemistry and Materials Science, Anhui Normal University, Wuhu 241000, China

Supporting Information

ABSTRACT: We prepared the Poly(*N*-vinylcarbazole)/sulfur@reduced graphene oxide (PVK/S@RGO) composites via a facile vibrating-emulsification synthesis method, which consist of the composites cores of large sulfur particles integrated into PVK conductive network and the conducting shell of reduced graphene oxide sheets. The PVK in the composites plays multiple roles in different processes. In preparation processes, PVK functions as dispersants to prevent sulfur particles from aggregating into excessively large size. And in the cycling test, PVK could play as additional electroactive binders and barriers to reinforce the electrode stability, accommodate volume change and reduce polysulfides shuttling. The resulting PVK/S@RGO composites containing 71 wt % sulfur exhibit excellent cycling performance and rate properties with a high discharge capacity of 843.5 mA h g^{-1} and a charge capacity retention of 77% (only 0.07% capacity degradation per cycle) from 20th to 400th at 1 *C*, corresponding to an average Coulombic efficiency of over 94%.

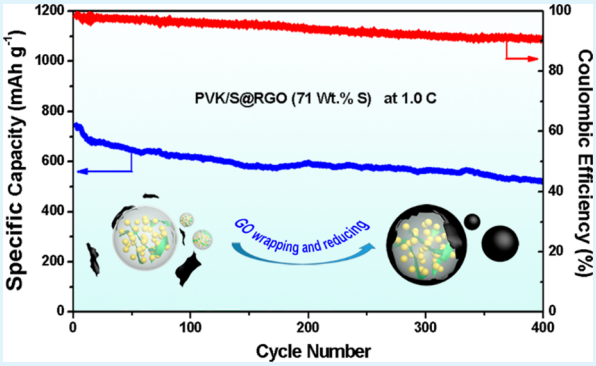

KEYWORDS: *poly(N-vinylcarbazole), graphene, lithium−sulfur battery, electrochemical performance, emulsification ratio, vibrating-emulsification synthesis method*

1. INTRODUCTION

High-energy-density batteries have been a great demand in the field of new energy vehicles. Traditional lithium-ion batteries cannot meet the requirements of electric vehicles (EV) and hybrid electric vehicles (HEV) because of their limited theoretical capacity.[1−3] Lithium−sulfur (Li−S) batteries have been widely considered as appealing candidates for the next generation of high-energy-density batteries,[4] because of their high theoretical energy density of 2600 W h kg^{-1}, high specific capacity of 1675 mA h g^{-1},[5,6] inexpensive cost, and the fact they are environmentally benign.[7,8] However, the practical applications of Li−S batteries have been plagued by the following problems: (1) sulfur is both ionically and electrically insulating (5×10^{-30} S cm^{-1} at 25 °C),[4] giving rise to low sulfur utilization and poor rate performance; (2) the high-order lithium polysulfides (Li_2S_n, $4 \leqslant n \leqslant 8$) are of high solubility and diffusivity, resulting in a "shuttling" phenomenon of the diffusion back and forth between the anode and cathode and thus leading to rapid capacity fading;[9,10] (3) the insoluble low-order lithium polysulfides and final discharge products (Li_2S_2 and Li_2S) can precipitate on the surface of electrodes and decrease the contact area between electrolyte and active materials;[10] (4) a great volume expansion of sulfur during charge−discharge processes may destroy the structure of the electrode.[11,12] All these problems account for short cycle life, inferior rate capability, and low Coulombic efficiency of Li−S batteries.

To address above problems, various carbon materials such as porous carbon,[13−15] hollow carbon spheres,[9,16] carbon nanotubes,[17−19] carbon nanofibers[20,21] and conducting polymers such as polyaniline (PANI),[8,22] polypyrrole (PPy),[23] and poly(3,4-ethylenedioxythiophene) (PEDOT)[24,25] have been chosen as matrixs to integrate with nanosized sulfur. The electrochemical performances including the cycling life and rate capability have been improved to some extent because of the good electronic conductivity or adsorption capacity of the matrixs. Regrettably, the nanosized sulfur particles could not meet the industrial demands and suffer from many intrinsic defects. The advantages of the nanosized sulfur have been overemphasized, and their disadvantages have been neglected.[17,26,27] It has been well-known that the nanosized sulfur particles have a low tap density and thus resulting in a low volumetric energy density. And nanosized sulfur particles are relatively soluble and apt to dissolve the polysulfide, leading to poor cycling ability.[24] Furthermore, coating ultrafine sulfur nanoparticles with high specific surface area needs more

Received: May 19, 2015
Accepted: July 8, 2015
Published: July 8, 2015

DOI: 10.1021/acsami.5b04079
ACS Appl. Mater. Interfaces 2015, 7, 16668−16675

conducting materials, which may be adverse to further increasing sulfur content. The volumetric energy density, cycling ability, and sulfur content are so critical to practical application of Li−S batteries.

On the other hand, micrometer-sized sulfur particles are generally hard to fulfill their electrochemical potential because of the intrinsically poor electronic conductivity of sulfur. Some efforts of wrapping large sulfur with conducting materials have been devoted to make better use of large sulfur. The composites of wrapping micrometer sulfur with carbon black decorated mildly oxidized graphene oxide sheets have shown high capacity and cycling stability.[28] The core−shell sulfur-polypyrrole composites with micronmeter-sized sulfur demonstrate superior electrochemical stability and rate capability.[29] Despite there are some attempts to wrap large sulfur with conducting shells, little attention has been put on the internal connection between the large insulating sulfur cores and the contact between the cores and the shells.

To the best of our knowledge, the poly(*N*-vinylcarbazole)/sulfur wrapped by reduced graphene oxide as electrode materials of stable high-performance lithium−sulfur batteries have not been reported yet. Herein, we fabricate poly(*N*-vinylcarbazole)/Sulfur@Reduced Graphene Oxide (PVK/S@RGO) composites with improved cycling and rate performances via a simple vibrating-emulsification synthesis method, which consist of the composites cores of large sulfur particles integrated into PVK conductive network and the conducting shell of reduced graphene oxide sheets. PVK is used to internally connect the insulating sulfur cores and bridge the contacting gap between cores and shells. The PVK/S@RGO composites with high sulfur content of 71 wt % made from different emulsification ratio of water to CS_2 (2:1, 3:1, and 4:1 in volume) are characterized and compared. The results suggest that the emulsification ratio of water to CS_2 has a crucial influence on the electrochemical performance of the products. The resulted PVK/S@RGO composites made from emulsification ratio of 3:1 show better electrochemical performances, which give a discharge capacity of 1318.7 mA h g^{-1}, 988.7 mA h g^{-1}, 839.2 mA h g^{-1}, and 525.9 mA h g^{-1} at 0.1, 0.5, 1, and 2 *C*, respectively. Meanwhile, a charge capacity retention of 77% and a high Coulombic efficiency of over 94% are obtained from 20th to 400th cycles at 1 C. Furthermore, the PVK plays multiple roles in different procedures. In preparation processes, PVK functions as a dispersant to prevent sulfur particles from aggregating into excessively large size. And in the charge−discharge processes, the PVK in electrode not only plays as additional electroactive binders to reinforce the electrode stability and accommodate volume changes, but also works as barriers to reduce polysulfide shuttling. Our work provides a simple and effective way to enable the micrometer-sized sulfur to release its excellent electrochemical performances for Li−S batteries.

2. EXPERIMENTAL SECTION

2.1. Preparation of Graphene Oxide (GO). Graphite oxide was prepared from oxidizing natural graphite powder by a modified Hummers' method.[30] First, 1 g of graphite powder and 0.5 g of sodium nitrate ($NaNO_3$) were added into 70 mL of concentrated H_2SO_4 in an ice bath, followed by the addition of 3 g of $KMnO_4$. The mixture was stirred and then diluted with deionized water. After that, 30% H_2O_2 was added into the solution until the color of the mixture became brilliant yellow. Repeated washing and centrifugation were performed to clean out the residual salt. Finally, solid graphite oxide was collected by freeze-drying. The as-prepared graphite oxide was ultrasonically dispersed in deionized water to obtain graphene oxide aqueous solution.

2.2. Preparation of PVK/S@RGO Composites. Required amounts of GO aqueous solution were diluted into 4 mL, 6 and 8 mL, respectively, then ascorbic acid (VC) was added to these diluted GO solution (in a weight ratio of VC/GO = 1:1) to prepare aqueous phase systems ($GO/VC/H_2O$). Oil phase system($S/PVK/CS_2$) was made through dissolving sulfur (≥99.5%, AR, Chengdu Kelong Chemical Reagent Co., China) and PVK (M_n = 25 000−50 000, Sigma-Aldrich) powder (5:1 w/w) in carbon disulfide (CS_2) under magnetic stirring at room temperature. Oil phase systems without PVK addition (S/CS_2) are also prepared in the same procedure for comparison. Next, aqueous phase systems ($GO/VC/H_2O$) with constant mass of GO and VC in different volume were dropped into the as-prepared oil phase systems ($S/PVK/CS_2$ or S/CS_2), followed by tempestuously vibrating to form oil-in-water emulsions and then slowly heating them to 90 °C and keeping at the temperature for 4.5 h under constant stirring. The final products were collected by vacuum filtrating and lyophilization.

2.3. Material Characterization. The morphology analysis and elements distribution were conducted on a scanning electron microscope (SEM, Carl Zeiss SMT Pte Ltd., Ultra 55) and a transmission electron microscope (TEM, Carl Zeiss SMT Pte Ltd., Libra 200 FE, 200 kV) that is equipped with energy-dispersive spectroscope (EDS). The crystalline structure of samples was characterized by X-ray diffraction (XRD) using a Bruker DX-1000 diffractometer with Cu kα aradiation in the 2θ angular range of 10−80° at a scanning rate of 0.08° per second. Fourier transform infared (FTIR, PerkinElmer Instrument Co.) spectra were recorded by a PerkinElmer spectrum two in the wavenumber range of 4000−500 cm^{-1}. The content of sulfur in the as-prepared PVK/S@RGO composites was determined by a Thermogravimetric analysis (TGA, METTLER) in a temperature range of 35−750 °C in nitrogen atmosphere at a heating rate of 10 °C per minute.

2.4. Electrochemical Measurements. Coin-type (CR2032) cells were assembled in an Ar-filled glovebox to evaluate the electrochemical performance of the PVK/S@RGO composites as cathode materials for Li−S batteries. The PVK/S@RGO (or S@RGO) cathode slurry was prepared by mixing the PVK/S@RGO (or S@RGO) composites (70%), acetylene black (20%) and polyvinylidene fluoride (PVDF) (10%) in *N*-methylpyrrolidone (NMP). Positive electrodes were produced by coating the slurry onto aluminum foil and drying at 60 °C for 12 h. Then the aluminum foil was cut into circular discs and the areal density of the electrode was in the range of 1.6−1.9 mg cm^{-1}. The electrolyte used was 1 M LiTFSI in a solvent mixture of DOL/DME (1:1 v/v) with 0.5 wt % $LiNO_3$ addition.[31] Lithium metal foil was used as the counter electrode and Celgard 2400 as separators. The coin cells were tested in galvanostatic mode at various currents within a voltage range of 1.5−2.8 V using the CT2001A battery program controlling test system (China-Land Co., Ltd.). The cyclic voltammogram (CV) and electrochemical impedance spectroscopy (EIS) measurements were performed on a VSP (Bio-Logic SAS) electrochemical workstation with a voltage from 1.0 to 3.0 V (Li^+/Li) at a scan rate of 0.2 mV s^{-1} and amplitude of 10 mV in frequency range of 100 kHz to 10 mHz, respectively. A current density of 1600 mA h g^{-1} (1.0 C) based on the mass of sulfur, which is equivalent to full discharge or charge in 1 h, was applied in both current sweep directions. The capacities were calculated on the basis of the mass of sulfur.

3. RESULTS AND DISCUSSION

The main synthesis processes of PVK/S@RGO composites are illustrated in Figure 1. First, aqueous phase systems ($GO/VC/H_2O$) are dropped into the as-prepared oil phase systems ($S/PVK/CS_2$), followed by vigorously vibrating to form oil-in-water emulsions and then slowly heating them to drive CS_2 away. Finally, vacuum filtrating and freeze-drying are applied to obtain the PVK/S@RGO composite. Unlike simple mixing method that put the core materials and the shell materials in

DOI: 10.1021/acsami.5b04079
ACS Appl. Mater. Interfaces 2015, 7, 16668−16675

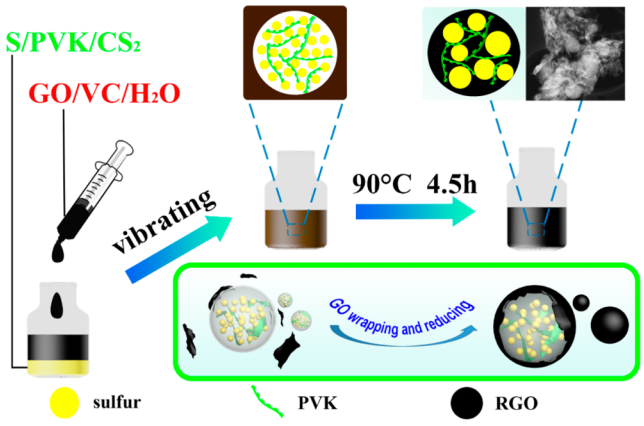

Figure 1. Schematic illustration of the preparation of PVK/S@RGO composites.

the same phase, this vibrating-emulsification synthesis method separates the core from the shell by putting them in water phase and oil phase, respectively, which could significantly increase the wrapping efficiency. More importantly, this method combines both the outer conducting shells of graphene and the internal connection network of PVK with insulating sulfur cores at the same time.

The size of final sulfur particles is influenced by the emulsification ratio of the water phase to oil phase (W:O). A low emulsification ratio means large CS_2 drops containing more sulfur suspending in small amount of water containing the grapheme oxide. When CS_2 is evaporated up, larger PVK/S composite particles are precipitated and graphene oxide in the water simultaneously tends to aggregate and coat on the PVK/S composites due to the hydrophilic properties. Despite in the evaporation processes of CS_2 and the precipitation process of sulfur, the PVK in the CS_2 drops functions as a dispersant to prevent the sulfur particles from aggregating to some extent. Large CS_2 drops still produce relatively larger PVK/S composite particles, because larger CS_2 drops contain more sulfur and PVK. However, a high emulsification ratio is also undesirable, because PVK is highly hydrophobic and thus easily precipitates with sulfur from the water-rich oil-in-water system during the heating process, resulting in failure in wrapping RGO on sulfur particles. The microstructures of PVK/S@RGO composites prepared from different emulsification ratios are characterized by SEM as shown in Figure 2. It can be seen that the emulsification ratio of W:O has a crucial influence on the morphologies of PVK/S@RGO composites. For low emulsification ratio (2:1), PVK/S particles are wholly encapsulated by RGO shells to assemble into excessively large PVK/S@RGO composites, as shown in Figure 2a, d. For higher emulsification ratio (4:1), a lot of bare nanoparticles are observed (Figure 2c, f). This is because hydrophobic PVK tends to precipitate with sulfur in the water-rich system before graphene wrapping. For the ratio of 3:1, sulfur particles integrated with PVK are uniformly wrapped by RGO shell with a size of about 5 μm. As shown in Figure 2b, e, no bare sulfur nanoparticles can be found on the surface of the composites. It can be seen from the SEM images that the emulsification ratio of 3:1 can produce effective wrapping with moderate size.

TEM images of the PVK/S@RGO composites made from the emulsification ratio of 3:1 are shown in Figure 3a, b. The

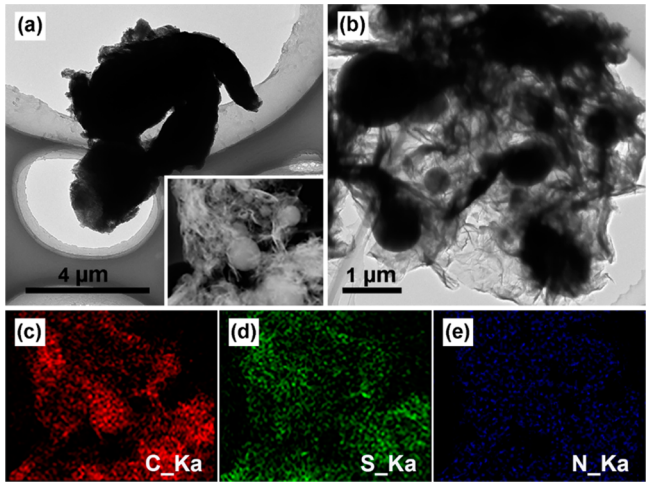

Figure 3. (a, b) TEM images of PVK/S@RGO composites made from an emulsification ratio of 3:1. The inset is the image of scanning transmission electron microscopies of the PVK/S@RGO composites. Elemental mapping of (c) carbon, (d) sulfur, and (e) nitrogen in the PVK/S@RGO composites.

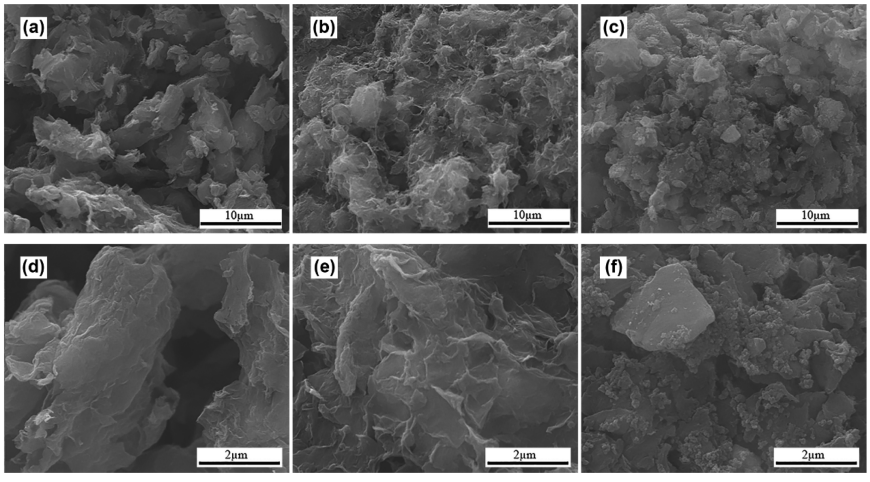

Figure 2. SEM images of PVK/S@RGO composites made from different emulsification ratios: (a, d) 2:1, (b, e) 3:1, and (c, f) 4:1.

DOI: 10.1021/acsami.5b04079
ACS Appl. Mater. Interfaces 2015, 7, 16668−16675

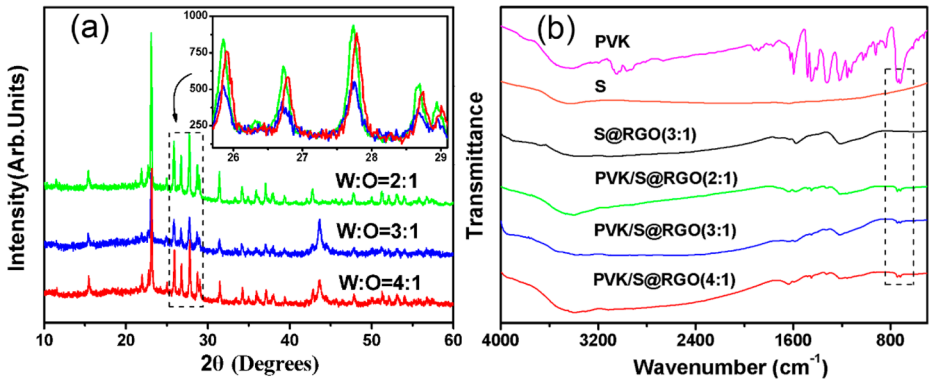

Figure 4. (a) XRD patterns of PVK/S@RGO composites. (b) FTIR spectra of pure PVK, pure S, S@RGO composites and PVK/S@RGO composites.

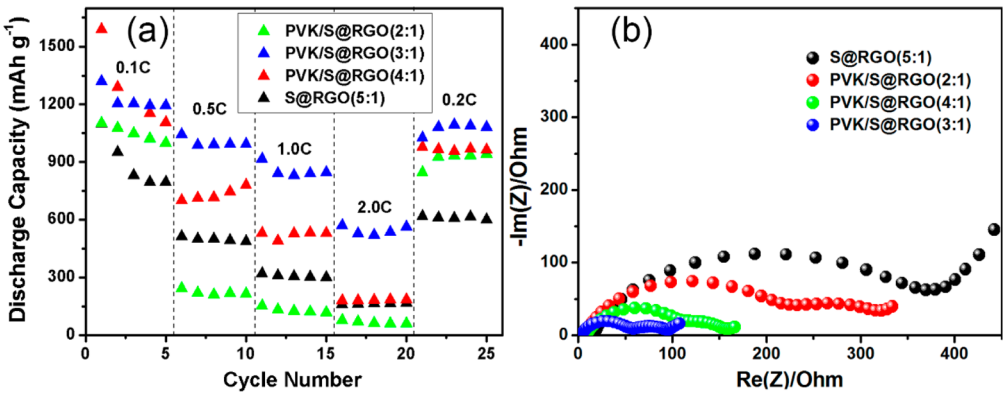

Figure 5. (a) Rate capabilities and (b) Nyquist plots of the electrode for S@RGO composites and PVK/S@RGO composites.

PVK/S@RGO composites consist of the spheres combining the sulfur with PVK as the core coated with RGO as the shell. Figure 3c–e show the elemental mapping of carbon, sulfur and nitrogen in the inset in Figure 3a, respectively. It can be seen that all the carbon, sulfur and nitrogen are uniformly distributed in the PVK/S@RGO composites. Because only the PVK molecule contains nitrogen element in the composites, the nitrogen elemental mapping could well reflect the existence and distribution of the PVK in the PVK/S@RGO composites. The results demonstrate the uniform distribution of PVK in the composites.

To further study the effect of emulsification ratios on the structure and composition of the composites, XRD of pure sulfur, S@RGO and PVK/S@RGO composites were conducted as shown in Figure S1 (in the Supporting Information) and Figure 4a. All patterns have two prominent peaks at approximately 23 and 28° (2θ), corresponding to an *Fddd* orthorhombic structure of sulfur.[11] Compared with the patterns of pure sulfur and S@RGO in Figure S1 in the Supporting Information, the XRD spectra of PVK/S@RGO(2:1), PVK/S@RGO(3:1) and PVK/S@RGO(4:1) do not exhibit any obviously new peaks except slightly shifting of the peak position as displayed in the inset in Figure 4a due to the amorphous phase of PVK polymer. The patterns for the graphene at approximately 26° could not be observed in the S@RGO and PVK/S@RGO composites because of the strong diffraction peaks from the highly crystalline sulfur and low content graphene.

FTIR were also conducted on pure sulfur, pure PVK, S@RGO composites and PVK/S@RGO composites, respectively (Figure 4b). For the pure PVK, strong peaks at 750–2000 cm^{-1} and the broad peak at 3050–2920 cm^{-1} can be observed, which are associated with C–H stretching vibrations of aryl groups.[32] For the pure S, it presents a continuous strip without obvious absorption peaks from 500 to 4000 cm^{-1}. For all the PVK/S@RGO composites, the characteristic absorption banding of the carbazole group in PVK molecule can be observed at 751 and 725 cm^{-1},[33,34] but the two peaks could not be found in the S@RGO composites.

The sulfur content in the PVK/S@RGO composites is determined by TGA. As seen in Figure S2 in the Supporting Information, the content of sulfur declines from 100% at about 155 °C to 0% before 300 °C. In the same range, the PVK decreases 7.8% of its weight, assigning to its transition point.[35] For the PVK/S@RGO composites, it can be known that the first decline can be attributed to the loss of whole sulfur weight and 7.8% weight loss of the PVK in the composites. While the second decline between 300 and 500 °C can be contributed to the loss of the remaining weight of PVK. Calculated based on these TGA profiles, the mass fractions of PVK, RGO and sulfur in the PVK/S@RGO composites are 11.17, 17.41, and 71.42%, respectively.

For simplicity, the electrodes made from PVK/S@RGO composites (2:1, 3:1, and 4:1) are referred as PVK/S@RGO-2, PVK/S@RGO-3, and PVK/S@RGO-4, respectively. Electrochemical measurements were carried out to evaluate the electrochemical performances of PVK/S@RGO composites. It can be seen from Figure 5a that the emulsification ratios markedly influence the rate capabilities of PVK/S@RGO composites. The PVK/S@RGO-4 shows the highest initial

DOI: 10.1021/acsami.5b04079
ACS Appl. Mater. Interfaces 2015, 7, 16668–16675

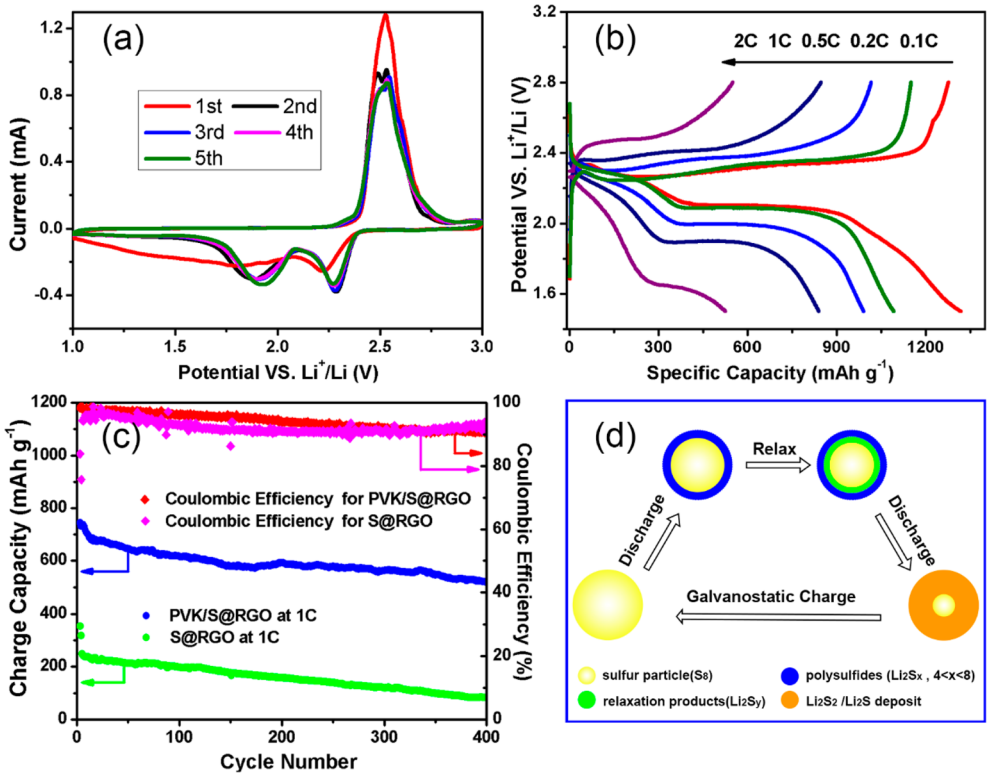

Figure 6. (a) CV curves and (b) galvanostatic charge/discharge profiles of the PVK/S@RGO-3. (c) Cycling performances of the PVK/S@RGO-3 and S@RGO(5:1) electrode. (d) Schematic illustration of charge/discharge and relaxation processes.

discharge capacity, but it decreases rapidly during the first 5 cycles. The rapid decay of capacity may be assigned to the diffusion resistance of bare sulfur nanoparticles without effectively wrapping which can be seen in Figure 2c, f, whereas the PVK/S@RGO-2 reveals poor rate performances because of the excessively large size of PVK/S@RGO(2:1) composites. The PVK/S@RGO-3 shows the best rate capabilities and cycle stability. To demonstrate the indispensability of PVK in this vibrating-emulsification synthesis method, we carried out another series of experiments without PVK in different emulsification ratios. Figure S3 in the Supporting Information shows the rate capabilities of the S@RGO composites made from different emulsification ratios (2:1, 3:1, 4:1, and 5:1). Compared with the PVK/S@RGO, it can be seen that all the S@RGO present a relatively poor rate capability, which demonstrates that the PVK in the composites could facilitate the improved electrochemical performances of the large sulfur, ascribed to the formation of internal connection network.

Figure 5b shows the EIS of the S@RGO and the PVK/S@RGO obtained from different emulsification ratios. It can be seen that the Nyquist plots of the S@RGO are composed of one semicircle in the high-frequency (HF) region and an inclined line in the low-frequency (LF) region. For the PVK/S@RGO, two semicircles can be observed in the Nyquist plots. The semicircle in the HF region can be assigned to the charge transfer processes.[36] And the semicircle in the low-frequency (LF) region may be attributed to the reprecipitated PVK film on the surface of active materials. The diameter of the semicircle along the *X*-axis represents the resistance value, which is one of the important factors in electrochemical reactions.[37−39] It can be seen that the PVK/S@RGO-3 shows the smallest charge transfer resistance compared to the S@RGO, PVK/S@RGO-2 and PVK/S@RGO-4. The results demonstrate that without the dispersion and integration of PVK, the S@RGO composites have an increased charge-transfer resistance due to the larger sulfur particle size and poor interfacial conductivity.

To gain a further insight into the electrochemical performance of the PVK/S@RGO(3:1) composites, CV and galvanostatic charge/discharge testing are employed to explore the kinetic processes. The CV profiles of the PVK/S@RGO-3 are presented in Figure 6a. It can be seen that there are two cathodic peaks, corresponding to the formation of long-chain polysulfides (Li_2S_x, $4 \leqslant x \leqslant 8$) and short-chain Li_2S_2 and Li_2S.[40] Accordingly, two anodic peaks can be observed at approximately 2.45 and 2.55 V, corresponding to the oxidation of Li_2S to polysulfides and polysulfides to S_8. Followed by the increased cycles, the cathodic peaks and the anodic peaks are well-overlapped, which demonstrates a good reversibility and a cycling stability of the electrode.[41]

Figure 6b shows the galvanostatic charge/discharge curves of the PVK/S@RGO-3 at various current rates. Consistent with two cathodic peaks in the CV profiles, the discharge curves are composed of two plateaus. It can be seen that the composites can deliver a discharge capacity of 1318.7, 1092.8, 988.7, 839.2, and 525.9 mA h g^{-1} at 0.1, 0.2, 0.5, 1, and 2 *C*, respectively.

Long-term cycling test was carried out at 1 *C* to investigate the cycling stability of PVK/S@RGO-3. As shown in Figure 6c, the composites have a charge capacity of 743.9 mA h g^{-1}. Even after 400 cycles at a high current rate of 1 *C*, PVK/S@RGO-3 still delivers a high charge capacity of 517.6 mA h g^{-1} with an average Coulombic efficiency of over 94%, corresponding to 77% capacity retention with only 0.07% capacity degradation per cycle. While in the absence of PVK, the S@RGO(5:1) electrode has the highest charge capacity of only 354 mA h g^{-1} and a low charge capacity retention of only 35% from fifth to

DOI: 10.1021/acsami.5b04079
ACS Appl. Mater. Interfaces 2015, 7, 16668−16675

400th at 1 C. It can be speculated that during the charge−discharge processes, the PVK in the PVK/S@RGO composites not only plays as additional electroactive binders to reinforce the electrode stability and accommodate volume changes, but also works as barriers to reduce polysulfide shuttling.

In previous CV profiles, the reductive peak at a low potential of about 2.0 V corresponding to the reduction of soluble polysulfide anions to an insoluble low-order Li_2S_2/Li_2S deposit[42] is generally stronger than the high potential one. While our low potential reductive peak is depressed and located at a lower potential of 1.9 V. Here we provide a possible interpretation. Our sulfur particles in the electrode are relatively larger. While the elemental sulfur (S_8) on the sulfur particles surface is reduced to polysulfides (Li_2S_x, $4 \leqslant x \leqslant 8$) and some Li_2S_x is further reduced to Li_2S_2/Li_2S deposit, the internal elemental sulfur still exists in S_8 form as illustrated in Figure 6d. Relaxation reactions ($S_8 + Li_2S_2 + Li_2S \rightarrow Li_2S_y$) may occur in the interface region, where y is smaller than x. The interfacial relaxation reaction could increase sulfur utilization and lead to the depressed reductive peak at a lower potential in Figure 6a.

To investigate the existence of the relaxation reaction in large sulfur, we use a pure S electrode (preparation details are described in the Supporting Information) to charge−discharge at various current rates. As shown in Figure S4, the potential of the discharge curve at 0.5 *C* falls to 1.53 V and then slowly raises to 1.8 V and keeps at a low plateau to give a high discharge capacity. Since the potential of electrode is mainly determined by its chemical substances and a declining discharge curve corresponds to a process of high-order polysulfides to low-order polysulfides, therefore a rising discharge curve necessarily corresponds to a reverse process of low-order polysulfides to high-order polysulfides. According to the relaxation mechanism, we may explain the phenomena that the PVK/S@RGO-2 can only release desirable discharge capacities at a low current rate and cannot at a high current rate. At a high current rate, the electrochemical reaction rate is much faster than the relaxation reaction rate. When a large flux of Li^+ migrate to the surface of sulfur particle to fastly form a Li_2S layer which may block the diffusion of Li^+ into the interior of the particle. The internal sulfur does not have enough time to react with the insoluble Li_2S to form soluble Li_2S_y before the potentials reach the cutoff voltage. Therefore, PVK/S@RGO-2 electrodes without the effectively conductive network show a very low specific capacity at a high current rate. While at a low current rate, most of the sulfur could be utilized through the relaxation reaction to give desirable discharge capacities.

To better understand the improved cycling performance of PVK/S@RGO electrodes, we characterized the surface morphologies of the PVK/S@RGO-3 before cycling and after 400 cycles at 1 C. Compared with the electrode before cycling, the PVK/S@RGO-3 after 400 cycles still maintains good connection structure as shown in Figure 7a, b.

The excellent electrochemical performances of the PVK/S@RGO-3 derive from the comprehensive consideration of both the good outer conducting shells and the internal connection network. First, the PVK internally connects and integrates with large insulating sulfur particles. Meanwhile, RGO with good conductivity provides favorable outer conductive network. Such synergistic conduction forms a three-dimensional electronic network, which helps to promote the rate capabilities. Moreover, the PVK integrated with core sulfur particles not only plays as additional binders to reinforce the electrode stability and accommodate volume changes, but also serves as the first barrier to restrain polysulfide leaving. RGO shell acts as the second barriers to further minimize the polysulfide shuttling. In addition, a suitable size of the sulfur could realize the combination of electronic conductivity and high sulfur utilization.

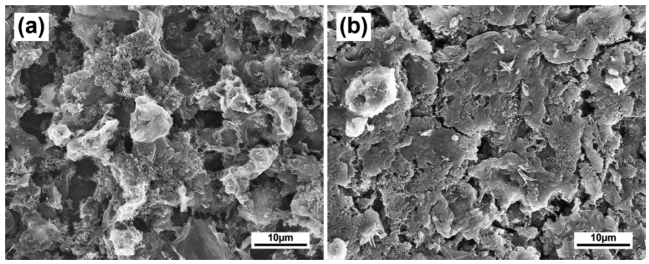

Figure 7. SEM images of the PVK/S@RGO-3: (a) the fresh electrode without pressing, (b) the electrode after 400 cycles at 1 C.

4. CONCLUSIONS

PVK/S@RGO composites with high S content were prepared via a facile vibrating-emulsification synthesis method. The emulsification ratio has a crucial influence on the morphology and electrochemical performance of the products. The composites prepared from the emulsification ratio of 3:1 show better performances compared with bare sulfur and S@RGO. The as-prepared PVK/S@RGO composites exhibit excellent electrochemical properties, including high specific capacity, good rate capability and high capacity retention. PVK in the composites plays multiple roles in the whole processes. In the emulsion process, PVK could function as dispersants to prevent sulfur particles from excessively aggregating. And in the cycling test, PVK could play as additional binders and barriers to reinforce the electrode stability, accommodate volume change, and reduce polysulfides shuttling.

■ ASSOCIATED CONTENT

Supporting Information

Fabrication of pure sulfur electrode, XRD patterns of pure S and S@RGO composites, TGA profiles of S, PVK and PVK/S@RGO composites, rate capabilities of the electrode for S@RGO composites made from different emulsification ratios, galvanostatic charge/discharge profiles of the pure S electrode. The Supporting Information is available free of charge on the ACS Publications website at DOI: 10.1021/acsami.5b04079.

■ AUTHOR INFORMATION

Corresponding Author

*Fax: +86 816 2544 426. E-mail: edward.bwang@gmail.com or binwang@caep.cn.

Author Contributions

†G.Q. and J.C. contributed equally to this work.

Notes

The authors declare no competing financial interest.

■ ACKNOWLEDGMENTS

This work was supported by the Applied Fundamental Foundation of Sichuan Province (2014JY0202), the R&D Foundation of China Academy of Engineering Physics (2014B0302036), National Natural Science Foundation of China (21401177), the "1000plan" from the Chinese Government, the Collaborative Innovation Foundation of SiChuan University (XTCX2014009), and the Natural Science Founda-

DOI: 10.1021/acsami.5b04079
ACS Appl. Mater. Interfaces 2015, 7, 16668−16675

tion of the Anhui Higher Education Institutions of China (KJ2012A126).

REFERENCES

(1) Barghamadi, M.; Best, A. S.; Bhatt, A. I.; Hollenkamp, A. F.; Musameh, M.; Rees, R. J.; Ruther, T. Lithium-Sulfur Batteries-the Solution Is in the Electrolyte, but Is the Electrolyte a Solution? *Energy Environ. Sci.* **2014**, *7*, 3902−3920.
(2) Lin, Z.; Liang, C. Lithium-Sulfur Batteries: From Liquid to Solid Cells. *J. Mater. Chem. A* **2015**, *3*, 936−958.
(3) Wang, Y.-X.; Huang, L.; Sun, L.-C.; Xie, S.-Y.; Xu, G.-L.; Chen, S.-R.; Xu, Y.-F.; Li, J.-T.; Chou, S.-L.; Dou, S.-X. Facile Synthesis of a Interleaved Expanded Graphite-Embedded Sulphur Nanocomposite as Cathode of Li−S Batteries with Excellent Lithium Storage Performance. *J. Mater. Chem.* **2012**, *22*, 4744−4750.
(4) Jayaprakash, N.; Shen, J.; Moganty, S. S.; Corona, A.; Archer, L. A. Porous Hollow Carbon@ Sulfur Composites for High-Power Lithium-Sulfur Batteries. *Angew. Chem.* **2011**, *123*, 6026−6030.
(5) Xi, K.; Cao, S.; Peng, X.; Ducati, C.; Kumar, R. V.; Cheetham, A. K. Carbon with Hierarchical Pores from Carbonized Metal−Organic Frameworks for Lithium Sulphur Batteries. *Chem. Commun.* **2013**, *49*, 2192−2194.
(6) Ji, L.; Rao, M.; Aloni, S.; Wang, L.; Cairns, E. J.; Zhang, Y. Porous Carbon Nanofiber-Sulfur Composite Electrodes for Lithium/Sulfur Cells. *Energy Environ. Sci.* **2011**, *4*, 5053−5059.
(7) Yang, Y.; Yu, G.; Cha, J. J.; Wu, H.; Vosgueritchian, M.; Yao, Y.; Bao, Z.; Cui, Y. Improving the Performance of Lithium−Sulfur Batteries by Conductive Polymer Coating. *ACS Nano* **2011**, *5*, 9187−9193.
(8) Zhou, W.; Yu, Y.; Chen, H.; DiSalvo, F. J.; Abruña, H. c. D. Yolk−Shell Structure of Polyaniline-Coated Sulfur for Lithium−Sulfur Batteries. *J. Am. Chem. Soc.* **2013**, *135*, 16736−16743.
(9) Zhang, C.; Wu, H. B.; Yuan, C.; Guo, Z.; Lou, X. W. D. Confining Sulfur in Double-Shelled Hollow Carbon Spheres for Lithium−Sulfur Batteries. *Angew. Chem.* **2012**, *124*, 9730−9733.
(10) Mikhaylik, Y. V.; Akridge, J. R. Polysulfide Shuttle Study in the Li/S Battery System. *J. Electrochem. Soc.* **2004**, *151*, A1969−A1976.
(11) Ji, X.; Lee, K. T.; Nazar, L. F. A Highly Ordered Nanostructured Carbon−Sulphur Cathode for Lithium−Sulphur Batteries. *Nat. Mater.* **2009**, *8*, 500−506.
(12) Lee, K. T.; Black, R.; Yim, T.; Ji, X.; Nazar, L. F. Surface-Initiated Growth of Thin Oxide Coatings for Li−Sulfur Battery Cathodes. *Adv. Energy Mater.* **2012**, *2*, 1490−1496.
(13) Schuster, J.; He, G.; Mandlmeier, B.; Yim, T.; Lee, K. T.; Bein, T.; Nazar, L. F. Spherical Ordered Mesoporous Carbon Nanoparticles with High Porosity for Lithium−Sulfur Batteries. *Angew. Chem., Int. Ed.* **2012**, *51*, 3591−3595.
(14) Chen, S.-R.; Zhai, Y.-P.; Xu, G.-L.; Jiang, Y.-X.; Zhao, D.-Y.; Li, J.-T.; Huang, L.; Sun, S.-G. Ordered Mesoporous Carbon/Sulfur Nanocomposite of High Performances as Cathode for Lithium−Sulfur Battery. *Electrochim. Acta* **2011**, *56*, 9549−9555.
(15) Lai, C.; Gao, X.; Zhang, B.; Yan, T.; Zhou, Z. Synthesis and Electrochemical Performance of Sulfur/Highly Porous Carbon Composites. *J. Phys. Chem. C* **2009**, *113*, 4712−4716.
(16) Brun, N.; Sakaushi, K.; Yu, L.; Giebeler, L.; Eckert, J.; Titirici, M. M. Hydrothermal Carbon-Based Nanostructured Hollow Spheres as Electrode Materials for High-Power Lithium−Sulfur Batteries. *Phys. Chem. Chem. Phys.* **2013**, *15*, 6080−6087.
(17) Jia-Jia, C.; Xin, J.; Qiu-Jie, S.; Chong, W.; Qian, Z.; Ming-Sen, Z.; Quan-Feng, D. The Preparation of Nano-Sulfur/Mwcnts and Its Electrochemical Performance. *Electrochim. Acta* **2010**, *55*, 8062−8066.
(18) Zhu, L.; Zhu, W.; Cheng, X.-B.; Huang, J.-Q.; Peng, H.-J.; Yang, S.-H.; Zhang, Q. Cathode Materials Based on Carbon Nanotubes for High-Energy-Density Lithium−Sulfur Batteries. *Carbon* **2014**, *75*, 161−168.
(19) Sun, L.; Li, M.; Jiang, Y.; Kong, W.; Jiang, K.; Wang, J.; Fan, S. Sulfur Nanocrystals Confined in Carbon Nanotube Network as a Binder-Free Electrode for High-Performance Lithium Sulfur Batteries. *Nano Lett.* **2014**, *14*, 4044−9.
(20) He, G.; Mandlmeier, B.; Schuster, J.; Nazar, L. F.; Bein, T. Bimodal Mesoporous Carbon Nanofibers with High Porosity: Freestanding and Embedded in Membranes for Lithium−Sulfur Batteries. *Chem. Mater.* **2014**, *26*, 3879−3886.
(21) Huang, L.; Cheng, J.; Qu, G.; Li, X.; Hu, Y.; Ni, W.; Yuan, D.; Zhang, Y.; Wang, B. Porous Carbon Nanofibers Formed in Situ by Electrospinning with a Volatile Solvent Additive into an Ice Water Bath for Lithium-Sulfur Batteries. *RSC Adv.* **2015**, *5*, 23749−23757.
(22) Ma, G.; Wen, Z.; Jin, J.; Lu, Y.; Wu, X.; Wu, M.; Chen, C. Hollow Polyaniline Sphere@Sulfur Composites for Prolonged Cycling Stability of Lithium-Sulfur Batteries. *J. Mater. Chem. A* **2014**, *2*, 10350−10354.
(23) Fu, Y.; Manthiram, A. Orthorhombic Bipyramidal Sulfur Coated with Polypyrrole Nanolayers as a Cathode Material for Lithium−Sulfur Batteries. *J. Phys. Chem. C* **2012**, *116*, 8910−8915.
(24) Chen, H.; Dong, W.; Ge, J.; Wang, C.; Wu, X.; Lu, W.; Chen, L. Ultrafine Sulfur Nanoparticles in Conducting Polymer Shell as Cathode Materials for High Performance Lithium/Sulfur Batteries. *Sci. Rep.* **2013**, *3*, 1910.
(25) Li, H.; Sun, M.; Zhang, T.; Fang, Y.; Wang, G. Improving the Performance of Pedot-Pss Coated Sulfur@Activated Porous Graphene Composite Cathodes for Lithium-Sulfur Batteries. *J. Mater. Chem. A* **2014**, *2*, 18345−18352.
(26) Shamsipur, M.; Pourmortazavi, S. M.; Roushani, M.; Kohsari, I.; Hajimirsadeghi, S. S. Novel Approach for Electrochemical Preparation of Sulfur Nanoparticles. *Microchim. Acta* **2011**, *173*, 445−451.
(27) Chen, H.; Wang, C.; Dong, W.; Lu, W.; Du, Z.; Chen, L. Monodispersed Sulfur Nanoparticles for Lithium−Sulfur Batteries with Theoretical Performance. *Nano Lett.* **2015**, *15*, 798−802.
(28) Wang, H.; Yang, Y.; Liang, Y.; Robinson, J. T.; Li, Y.; Jackson, A.; Cui, Y.; Dai, H. Graphene-Wrapped Sulfur Particles as a Rechargeable Lithium−Sulfur Battery Cathode Material with High Capacity and Cycling Stability. *Nano Lett.* **2011**, *11*, 2644−2647.
(29) Fu, Y.; Manthiram, A. Core-Shell Structured Sulfur-Polypyrrole Composite Cathodes for Lithium-Sulfur Batteries. *RSC Adv.* **2012**, *2*, 5927−5929.
(30) Kim, J.; Cote, L. J.; Huang, J. Two Dimensional Soft Material: New Faces of Graphene Oxide. *Acc. Chem. Res.* **2012**, *45*, 1356−1364.
(31) Zhao, Q.; Hu, X.; Zhang, K.; Zhang, N.; Hu, Y.; Chen, J. Sulfur Nanodots Electrodeposited on Ni Foam as High-Performance Cathode for Li−S Batteries. *Nano Lett.* **2015**, *15*, 721−726.
(32) Huang, L.; Cheng, J.; Li, X.; Yuan, D.; Ni, W.; Qu, G.; Guan, Q.; Zhang, Y.; Wang, B. Sulfur Quantum Dots Wrapped by Conductive Polymer Shell with Internal Void Spaces for High-Performance Lithium-Sulfur Batteries. *J. Mater. Chem. A* **2015**, *3*, 4049−4057.
(33) Xie, L.-H.; Ling, Q.-D.; Hou, X.-Y.; Huang, W. An Effective Friedel-Crafts Postfunctionalization of Poly (N-Vinylcarbazole) to Tune Carrier Transportation of Supramolecular Organic Semiconductors Based on Π-Stacked Polymers for Nonvolatile Flash Memory Cell. *J. Am. Chem. Soc.* **2008**, *130*, 2120−2121.
(34) Liu, G.; Zhang, B.; Chen, Y.; Zhu, C.-X.; Zeng, L.; Chan, D. S.-H.; Neoh, K.-G.; Chen, J.; Kang, E.-T. Electrical Conductivity Switching and Memory Effects in Poly (N-Vinylcarbazole) Derivatives with Pendant Azobenzene Chromophores and Terminal Electron Acceptor Moieties. *J. Mater. Chem.* **2011**, *21*, 6027−6033.
(35) Yao, M.; Senoh, H.; Sakai, T.; Kiyobayashi, T. Redox Active Poly (< I> N</I>-Vinylcarbazole) for Use in Rechargeable Lithium Batteries. *J. Power Sources* **2012**, *202*, 364−368.
(36) Yuan, L.; Qiu, X.; Chen, L.; Zhu, W. New Insight into the Discharge Process of Sulfur Cathode by Electrochemical Impedance Spectroscopy. *J. Power Sources* **2009**, *189*, 127−132.
(37) Arbizzani, C.; Catellani, M.; Mastragostino, M.; Mingazzini, C. N-and P-Doped Polydithieno [3, 4-B: 3′, 4′-D] Thiophene: A Narrow Band Gap Polymer for Redox Supercapacitors. *Electrochim. Acta* **1995**, *40*, 1871−1876.
(38) Yang, M. H.; Choi, B. G.; Park, H.; Hong, W. H.; Lee, S. Y.; Park, T. J. Development of a Glucose Biosensor Using Advanced Electrode Modified by Nanohybrid Composing Chemically Modified Graphene and Ionic Liquid. *Electroanalysis* **2010**, *22*, 1223−1228.

DOI: 10.1021/acsami.5b04079
ACS Appl. Mater. Interfaces 2015, 7, 16668−16675

(39) Wei, Y.-Z.; Fang, B.; Iwasa, S.; Kumagai, M. A Novel Electrode Material for Electric Double-Layer Capacitors. *J. Power Sources* **2005**, *141*, 386−391.
(40) Zhao, M. Q.; Zhang, Q.; Huang, J. Q.; Tian, G. L.; Nie, J. Q.; Peng, H. J.; Wei, F. Unstacked Double-Layer Templated Graphene for High-Rate Lithium-Sulphur Batteries. *Nat. Commun.* **2014**, *5*, 3410.
(41) Fu, Y.; Su, Y. S.; Manthiram, A. Highly Reversible Lithium/Dissolved Polysulfide Batteries with Carbon Nanotube Electrodes. *Angew. Chem., Int. Ed.* **2013**, *52*, 6930−6935.
(42) Yang, Z.; Guo, J.; Das, S. K.; Yu, Y.; Zhou, Z.; Abruña, H. D.; Archer, L. A. In Situ Synthesis of Lithium Sulfide−Carbon Composites as Cathode Materials for Rechargeable Lithium Batteries. *J. Mater. Chem. A* **2013**, *1*, 1433−1440.

DOI: 10.1021/acsami.5b04079
ACS Appl. Mater. Interfaces 2015, 7, 16668−16675